Navigating Materials Space with ML-Generated Electronic Fingerprints

Neporozhnii I[1], Wang Z[1], Bajpai R[1], Gómez C[1], Chakraborty N[1], Tamblyn I[2], Voznyy O[1,3*]

1. Department of Physical and Environmental Sciences, University of Toronto, Scarborough, 1065 Military Trail, Toronto, Ontario M1C 1A4, Canada
2. Department of Physics, University of Ottawa, 150 Louis-Pasteur Pvt, Ottawa, Ontario K1N 6N5, Canada
3. Lead Contact
* Correspondence: o.voznyy@utoronto.ca

Abstract:

In the field of materials science, finding materials with specific properties is a major challenge due to the vastness of the search space, which makes random exploration prohibitively expensive. A more practical approach is to search for new materials within the proximity of known compounds that possess the desired property. In such an approach, fingerprinting methods are often used to measure the similarity of materials and group them into clusters. Such methods rely exclusively on the material's structure to generate the fingerprint, which often does not correspond to clustering by desired property. To address this issue, electronic structure fingerprints that use properties such as the density of states (DOS) and band structure were proposed as an alternative. However, the computational cost of electronic structure calculations for tens of thousands of materials remains too high for rapid exploration. In this work, we developed a Graph Neural Network (GNN) ProDosNet which is trained on orbital Projected Density of States (PDOS) data and capable of predicting the electronic structure of materials at extremely low computational cost. With this model, we were able to generate PDOS fingerprints for all compounds present in the Materials Projects Database and cluster them by the similarity of their orbital PDOS, and therefore electronic properties. We demonstrate that using PDOS fingerprints allows finding materials that have similar electronic properties but drastically different structures.

Keywords:

Materials Discovery, Deep Learning, Graph Neural Networks, Density of States

Introduction:

The global transition to renewable energy sources requires advancements in photovoltaic (PV) devices and battery technology to meet the increasing demand for clean energy generation and storage. The performance of modern PV devices and batteries is mostly limited by the properties of materials used for their production. Furthermore, existing materials usually contain expensive and toxic elements which increase device prices and complicate their disposal, limiting accessibility and applications of clean energy technology.[1,2] Therefore, the discovery of new materials, especially lower-cost and free from heavy elements is necessary to facilitate successful transition from fossil-based fuels.

The discovery of inorganic materials for specific applications is complicated by the number of possible structures in the material space which is estimated to be on the order of 10^{12}.[3] The efficient exploration of such vast space requires methods beyond random sampling and heuristics. A much higher probability of finding promising materials can be achieved by creating a structured material space where compounds that possess similar properties are clustered together. If such structured material space is achieved, new materials can be sampled from the space around known state-of-the-art structures, increasing the probability of successful discovery.

In the field of organic chemistry, molecular fingerprints have been widely used to identify similar molecules and conduct virtual screening of the chemical space.[4–6] Molecular fingerprints are fixed-size vectors that encode information about molecular structure. After fingerprints are generated for all molecules in the dataset, similar structures can be found by comparing their fingerprints using metrics such as Tanimoto coefficient.[7] Recently, fingerprinting methods were applied to inorganic materials as well. The main disadvantage of the fingerprinting method is that it relies exclusively on the material's structure to generate fingerprints.

Electronic structure fingerprints that use properties such as Density of States (DOS) and band structure were proposed as an alternative to crystal structure fingerprints.[8] Incorporation of DOS and band structure information into fingerprint vector enables structurization of material space by electrochemical properties. However, the DOS fingerprinting approach relies on available electronic structure calculations to generate fingerprints. One of the largest publicly available databases of computed material properties – Materials Project Database contains information about 154,000 materials. However, only for 60% of these materials Density of States is calculated, which severely limits the electronic structure fingerprints approach.[9,10] It would be too slow to compute DOS for all of them using conventional methods, such as Density Functional Theory (DFT), and even more expensive to apply this approach to a larger space of compounds.

Machine learning (ML) models demonstrated prominent results in predicting materials properties such as formation energy, band gap, etc. Once trained, machine learning models can produce predictions with extremely low computational cost. Previous studies demonstrated that machine learning models can predict the total DOS of inorganic materials with sufficient accuracy and do not require significant computational resources.[11,12] However, these studies did not attempt to predict orbital densities, which are important for certain applications such as the discovery of battery cathode materials or catalysts. In this work, we propose to use the available DOS data to train a machine learning model capable of predicting orbital-resolved DOS and use these predictions to generate electronic fingerprints for all compounds in the materials space.

Methods:

Graph Neural Network

Graph Neural Networks (GNNs) is a subclass of machine learning algorithms designed for operating with graph representation of data. GNNs are widely used in the field of computational chemistry and material discovery due to the convenience of graph representation of material structures and leading performance in property prediction tasks. In this work, we developed a ProDosNet - GNN trained to predict PDOS of inorganic materials.

We use a modified version of Crystal Graph materials representation, which was first introduced along with the CGCNN model.[13] In Crystal Graph representation, the material is described by the set of nodes and edges. Nodes represent atoms in the unit cell and contain atomic descriptors, while edges represent bonds and provide information about interatomic distances and crystal geometry. In addition to the original Crystal Graph atomic descriptors, we also utilize s, p, and d atomic orbital energies, van der Waals radius, and ionic radius for each element. The x, y, and z components of interatomic distances were provided as bond features to enable the model to better capture the crystal geometry.

The model receives a graph representation of a crystal structure as input and produces output for each node of the graph. Node-level predictions correspond to orbital densities for each atom in the unit cell of the material. Such an approach allows us to predict and train on orbital densities – the most fundamental components of DOS. Using orbitally resolved data increases the number of training examples for each material by factor $\sigma = N_O \times N_A$ where N_O is a number of orbitals per atom and N_A is a number of atoms in the unit cell. The average factor $< \sigma >$ across the dataset is 227.5, resulting in more than 2 orders of magnitude increase in training information when using orbitally resolved data, compared to training on the total DOS.

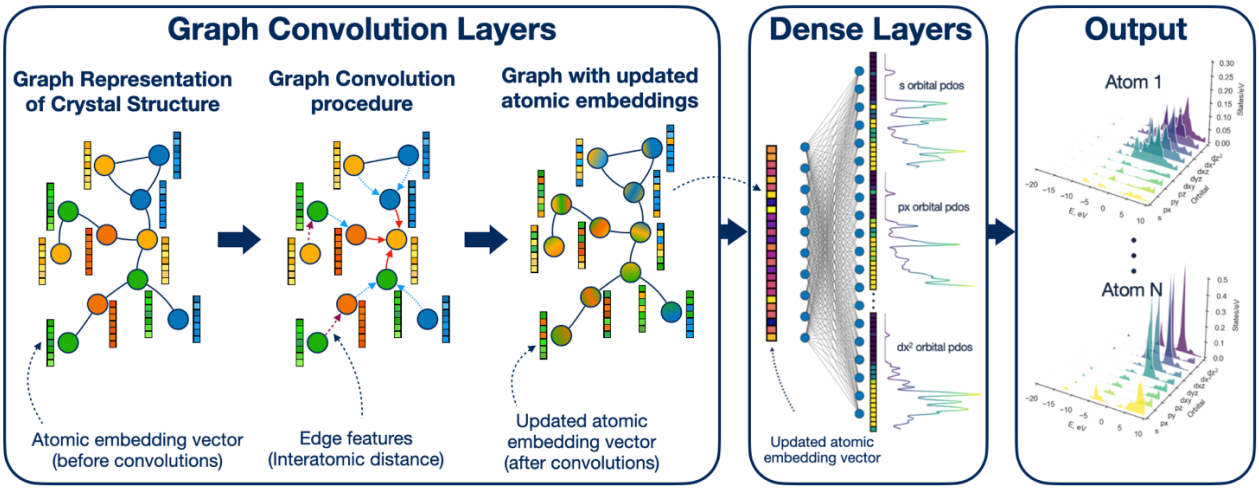

Figure 1. Schematic representation of ProDosNet model architecture. The first stage contains graph convolution layers which are responsible for the exchange of information between nodes and generation of updated atomic embedding vectors that contain information about atom's local environment (Equation 1). After the graph convolution layers, dense layers are used to obtain single orbital densities from updated atomic embedding vectors. The final output of the model is 9 orbital densities for each atom of the structure.

$$x_i' = x_i + \sum_{j \in U(i)} \lambda(x_i \oplus x_j \oplus e_{ij})$$

Equation 1. The convolution equation where x_i' represents the updated atomic embedding vector after convolution, x_i - initial atomic vector being concatenated with its atomic neighbors x_j and the bond information e_{ij} between them, and λ - multi-layer dense neural network.

Training the Model

One of the main challenges that arise when training a model to predict the Density of States is a choice of metric to measure the model performance. A minor misalignment in sharp density peaks can lead to high loss, even when the overall DOS prediction is accurate (Figure 2). Furthermore, standard loss functions such as RMSE or MAE do not capture improvement in PDOS prediction until target and predicted densities start to overlap, which can lead to poor performance for sharper density peaks. To overcome these issues, we used Wasserstein distance (also known as the earth mover's distance) as a metric to measure the accuracy of PDOS predictions. The Wasserstein distance between two distributions can be defined as and is equal to the area between their cumulative distribution functions (CDFs) (Equation 2). Using Wasserstein distance as a loss function allows us to account for the energy difference between predicted and target density peaks in addition to the PDOS amplitude difference at each grid point which is illustrated on a toy model example in the (Figure 2). This makes Wasserstein distance a better loss function to use for estimating the accuracy of PDOS predictions in comparison to more widely used RMSE and MAE. The Wasserstein distance is implemented as RMSE loss between PDOS CDFs. The PDOS can be obtained from predicted CDF by taking the derivative with respect to energy during the post-processing stage.

$$W_p(\alpha, \beta) = \left(\int_R \left|C_\alpha(x) - C_\beta(x)\right|^p dx\right)^{\frac{1}{p}}$$

Equation 2. The Wasserstein distance between two distributions can be defined as the area between their CDFs. Therefore, Wasserstein distance between two electronic densities of states can be computed as the area between DOS CDFs. In this study, factor p=2 is used.

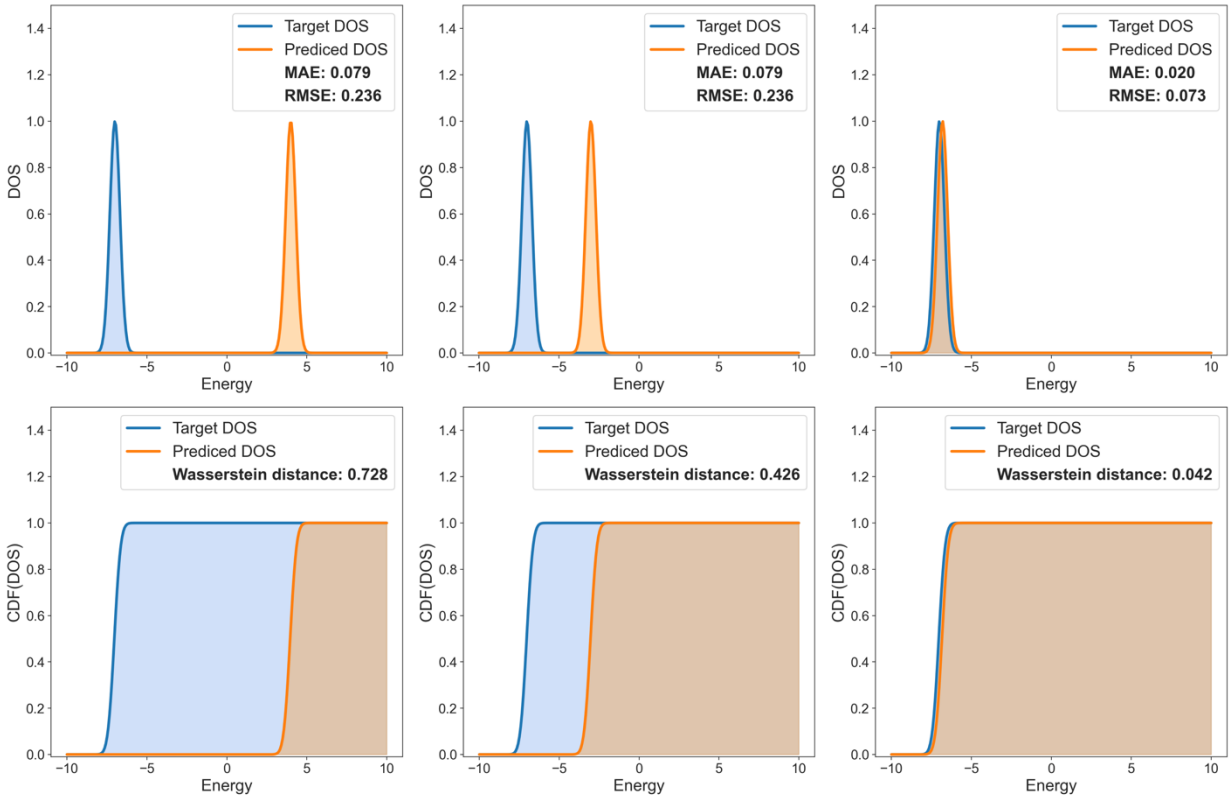

Figure 2. These plots illustrate on a toy model example how shifting the predicted density peak towards the target density peak does not change MAE or RMSE loss until the two densities start to overlap (A). In contrast, Wasserstein distance can capture the shift in predicted density peak, and therefore improves the predictions, regardless of how far the two peaks are located (B). This example demonstrates that Wasserstein distance is a more informative metric and should be used to measure the accuracy of DOS predictions.

PDOS fingerprints

The Density of States provides sufficient insight into material's electrochemical properties and can serve as a fingerprint to measure materials similarity. Furthermore, explicitly including s, p, and d orbital densities in the fingerprint vectors enables their use for applications where orbital-specific projections can play a crucial role.

To construct the fingerprint vector for each material we first predict its s, p, and d orbital densities. Each orbital density is represented as an amplitude on a 256-element energy grid which is defined by the ProDosNet model architecture. The total 768-element PDOS fingerprint vector is obtained by concatenation of s, p, and d orbital density vectors. Finally, the obtained PDOS fingerprint vector is normalized by the number of atoms in the unit cell.

To measure the similarity of PDOS vectors we use Wasserstein distance. Smaller Wasserstein distance indicates more similar PDOS, and therefore more similar electrochemical properties of materials. We can use the computed Wasserstein distance between available structures in the chemical space to cluster materials by the similarity of their PDOS.

Data availability and curation

Machine learning requires a substantial amount of data to train predictive models. We curated the PDOS dataset using crystal structures and DFT-calculated properties available in the Materials Project public database. Using Materials Project API, we obtained a CIF file and, if available, raw DOS data for each material in the database. During the preprocessing stage, we removed materials from the dataset that have spin-polarized calculations and contain elements with atomic number above 83. We also removed materials that have DOS but do not have full band structure calculations to avoid unreliable PDOS data. Furthermore, the VASP DFT software used to calculate material properties for the Materials Project database relies on a cutoff radius to project one-electron wavefunction onto spherical harmonic orbitals.[14–16] In the solid, radial components of atomic orbitals extend to infinity, potentially leading to projection overlap for neighbouring atoms. To overcome this issue, the cutoff radius for each element is used beyond which contributions are not included in the projections. The choice of cutoff radius is not a trivial task since the optimal value depends on specific environment. The non-optimal cutoff radius might result in orbital densities having incorrect projections due to double counting of contributions or not capturing all necessary contributions. Consequently, during data preprocessing, orbitals densities were renormalized to have an area equal to the number of states, and materials that contained orbitals densities with area significantly different from the number of states per orbital were removed from the training. For the remaining materials in the dataset, the Density of States data was preprocessed to a constant length DOS vector of size 256 using interpolation. The obtained DOS was then broadened using Gaussian filter with 0.3 eV standard deviation. The final dataset contains 23,140 materials. The 10% of the dataset were reserved for the test set and 90% were used for training and validation.

Results:

Predicting Projected Density of States

The ProDosNet architecture was specifically designed to enable prediction of DOS for every orbital of every atom in the material. The node-level predictions were achieved by removing a global pooling procedure and incorporating unembedding layers after graph convolution layers in the model. The node-level predictions can be later post-processed into s-orbital, p-orbital, d-orbital PDOS, atomic PDOS, element PDOS, and total DOS. The representative predictions illustrate the model's ability to predict various projections of DOS, including element- and orbital-specific components (Figure 3). Training with Wasserstein distance as a metric resulted in a significantly improved accuracy of predictions compared to RMSE or MAE (a detailed comparison of model's performance with different accuracy metrics is provided in SI). One of the most common errors encountered throughout the test set predictions is the overbroadening of sharp density peaks by the model.

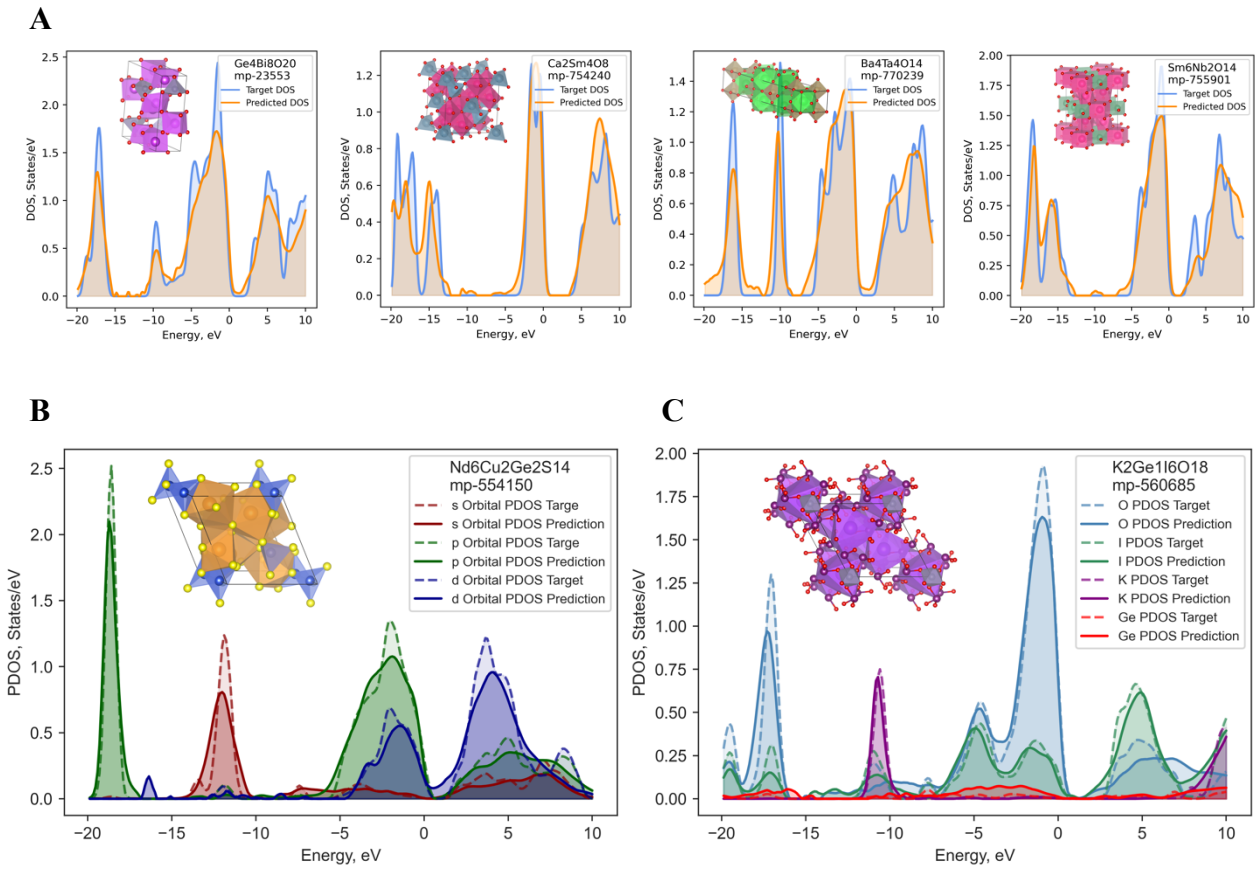

Figure 3. Randomly selected predictions on the test set with error within 5% of the median error. Total DOS predictions (A), orbital-projected DOS (B), and element-projected DOS (C).

Exploring Structured Materials Space

The trained ProDosNet model was used to predict PDOS for all materials in the Materials Project database, excluding compounds that contain radioactive elements, resulting in a total of 147,472 predictions. The predicted densities were used to generate PDOS fingerprints. To evaluate the applicability of a similarity-based search for new materials discovery, we evaluated four different applications: oxygen evolution catalysis, optoelectronics, solid-state ionic conductors, and Li-ion battery cathodes, using the known state-of-the-art materials as a starting point in each category: IrO_2, GaAs, $Li_{10}GeP_2S_{12}$, and $LiFePO_4$, respectively. The neighbours were selected from the list of the top 25 most similar stable materials by their predicted PDOS (Figure 4).

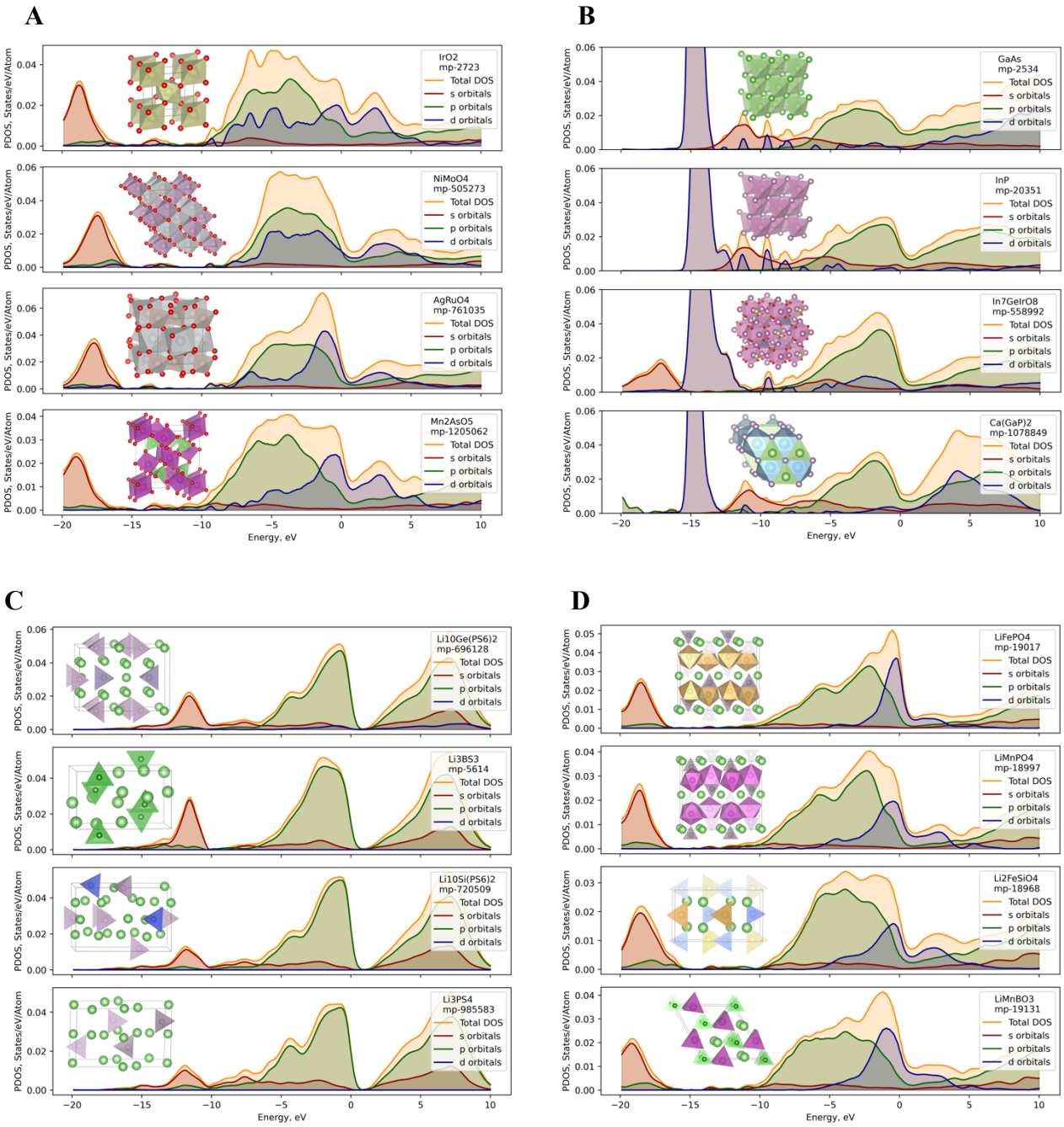

Figure 4. Each column shows a target material and 3 neighbours suggested by the model based on the PDOS similarity. Neighbours are sorted from most similar (first) to least similar (last).

IrO_2 is one of the best-known catalysts for OER in acidic solution.[17] Before the advanced DFT methods were developed for measuring the thermodynamic energy barriers for each proton-electron transfer reaction step as well as for surface Pourbaix diagrams calculations, a d-band center was previously used as an empirical metric of the catalyst activity, which supports the idea that electronic structure fingerprints, and specifically the one that distinguishes s, p, and d orbitals

is potentially a comprehensive descriptor not only for catalytic activity but also for material stability in acid.[18] The suggested neighbours with similar PDOS are $NiMoO_4$, $AgRuO_4$, and Mn_2AsO_5. An additional imposed requirement was that only metallic materials were selected to ensure better electrical conductivity. The manganese oxides are actively studied as potential electrocatalysts for OER, therefore, the presence of As-doped MnO is not unexpected and might additionally provide better stability and activity.[19] Among similar materials, we also observe Ag-doped RuOx, which is similar to Rb-doped IrOx, which is also present in the list of neighbors, and both provide better similarity than pure RuOx or RhOx – common replacements for IrOx. Indeed, while the overall shape of PDOS is similar between Ru and Ir oxides, their Fermi level positions are quite different, explaining that other materials provide closer similarity. $NiMoO_4$ provides the closest similarity to IrO_2, and is a low-component material that looks like an underexplored but promising OER catalyst.

The gallium arsenide is a well-studied semiconductor material commonly used in the production of photovoltaic devices, LEDs, and photodetectors. The primary properties of interest, optical bandgap and transition dipole moment can well be captured by the PDOS. Moreover, it is important to distinguish s, p, and d orbitals, as the valence and conduction bands should have different symmetry of the orbitals in order to allow for angular momentum change that enables optically-allowed electronic transitions. Some of the nearest neighbours of GaAs by predicted PDOS are InP, GaP, InAs and their alloys, which are also technologically popular semiconductors with similar properties. The other two close neighbours are In_7GeIrO_8 and $Ca(GaP)_2$, both of which are experimentally known. (A longer list of neighbors is provided in SI).

Solid-state inorganic electrolytes facilitate the emergence of new technologies including solid-state batteries and solid oxide fuel cells.[20,21] While the ionic conductivity seems to be purely defined by the crystal symmetry, such as the availability of empty sites for ion diffusion and Li-anion bond lengths, we hypothesize and argue that PDOS can potentially capture these properties indirectly. Specifically, the coordination number of Li ions and their coupling strength to the anionic lattice will inevitably affect the broadening of the original Li orbitals, which can be captured by the PDOS. To test this, we explored the neighbors of $Li_{10}GeP_2S_{12}$ - an electrolyte with one of the highest reported Li ionic conductivities.[22] The list of its PDOS neighbours includes $Li_{10}Si(PS_6)_2$, and Li_3PS_4 - two well-known decently-conducting electrolytes, and Li_3BS_3 – a material with a similar crystal and electronic structure.[22,23]

Lithium-ion batteries (LIBs) are dominant in the market of consumer electronics and begin to power electrification of the transportation sector, but their price and performance require further advances to be competitive and surpass the combustion engine[24]. The chemical stability of LIB cathodes is commonly represented through the PDOS where metal and oxygen orbitals determine the maximum voltage achievable before oxygen evolution happens. Therefore, PDOS can serve as a proxy to evaluate the suitability of materials as cathodes. As a starting structure, we use $LiFePO_4$ (LFP) - a widely used cathode material. Among the nearest neighbours of LFP by PDOS similarity are $LiMnPO_4$, $LiMnBO_3$, and Li_2FeSiO_4 all of which are actively studied as promising cathode materials for LIBs[25–29]. This demonstrates that the utilization of PDOS fingerprints led to the clustering of perspective cathode materials and successfully created a subspace of potentially valid compounds for further exploration.

Conclusions:

We demonstrate that ML-generated PDOS fingerprints can be used to create a structured material space where compounds that possess similar properties, and not just structural or compositional features, are clustered together. The presented examples illustrate the versatility of ML-generated PDOS fingerprinting approach across a wide array of applications. These include but not limited to discovery of novel catalysts, battery cathode materials, solid electrolytes, and photovoltaic materials. Furthermore, the proposed approach can be extended to a much larger material space with low additional computational cost. The PDOS fingerprinting approach has the potential to become a valuable tool for high-throughput material exploration by providing application-specific pool of promising materials to validate with more expensive computational or experimental techniques.

Code and Data Availability:

The code and data for this study are available at https://github.com/ineporozhnii/pdos_gnn

Acknowledgements:

This work was supported by the Natural Sciences and Engineering Research Council of Canada (NSERC CRD grant number 537463-18 and NSERC Discovery 2019-04897). Part of this work was sponsored by Huawei Canada. This research was enabled in part by support provided by Compute Ontario (https://www.computeontario.ca) and the Digital Research Alliance of Canada (alliancecan.ca). We thank Ted Sargent for fruitful discussions.

Author Contributions:

Conceptualization: I.N. and O.V.; Methodology: I.N. and O.V.; Software: I.N; Data acquisition: I.N. and Z.W.; Model development: I.N., R.B.; Analysis of predictions: I.N., C.G. N.C.; Investigation: I.N.; Writing Original Draft, Review and Editing: I.N. and O.V.; Supervision O.V.; Funding Acquisition O.V.

Declaration of Interests:

The authors declare no competing interests.

References:

(1) Lithium-Ion Batteries Need to Be Greener and More Ethical. *Nature* **2021**, *595* (7865), 7–7. https://doi.org/10.1038/d41586-021-01735-z.

(2) Olivetti, E. A.; Ceder, G.; Gaustad, G. G.; Fu, X. Lithium-Ion Battery Supply Chain Considerations: Analysis of Potential Bottlenecks in Critical Metals. *Joule* **2017**, *1* (2), 229–243. https://doi.org/10.1016/j.joule.2017.08.019.

(3) Walsh, A. The Quest for New Functionality. *Nat. Chem.* **2015**, *7* (4), 274–275. https://doi.org/10.1038/nchem.2213.

(4) Rogers, D.; Hahn, M. Extended-Connectivity Fingerprints. *J. Chem. Inf. Model.* **2010**, *50* (5), 742–754. https://doi.org/10.1021/ci100050t.

(5) Cereto-Massagué, A.; Ojeda, M. J.; Valls, C.; Mulero, M.; Garcia-Vallvé, S.; Pujadas, G. Molecular Fingerprint Similarity Search in Virtual Screening. *Methods* **2015**, *71*, 58–63. https://doi.org/10.1016/j.ymeth.2014.08.005.

(6) Willett, P. Similarity-Based Virtual Screening Using 2D Fingerprints. *Drug Discov. Today* **2006**, *11* (23), 1046–1053. https://doi.org/10.1016/j.drudis.2006.10.005.
(7) Fligner, M. A.; Verducci, J. S.; Blower, P. E. A Modification of the Jaccard–Tanimoto Similarity Index for Diverse Selection of Chemical Compounds Using Binary Strings. *Technometrics* **2002**, *44* (2), 110–119. https://doi.org/10.1198/004017002317375064.
(8) Isayev, O.; Fourches, D.; Muratov, E. N.; Oses, C.; Rasch, K.; Tropsha, A.; Curtarolo, S. Materials Cartography: Representing and Mining Materials Space Using Structural and Electronic Fingerprints. *Chem. Mater.* **2015**, *27* (3), 735–743. https://doi.org/10.1021/cm503507h.
(9) *Commentary: The Materials Project: A materials genome approach to accelerating materials innovation | APL Materials | AIP Publishing*. https://pubs.aip.org/aip/apm/article/1/1/011002/119685/Commentary-The-Materials-Project-A-materials (accessed 2023-08-27).
(10) Munro, J. M.; Latimer, K.; Horton, M. K.; Dwaraknath, S.; Persson, K. A. An Improved Symmetry-Based Approach to Reciprocal Space Path Selection in Band Structure Calculations. *Npj Comput. Mater.* **2020**, *6* (1), 1–6. https://doi.org/10.1038/s41524-020-00383-7.
(11) Kong, S.; Ricci, F.; Guevarra, D.; Neaton, J. B.; Gomes, C. P.; Gregoire, J. M. Density of States Prediction for Materials Discovery via Contrastive Learning from Probabilistic Embeddings. *Nat. Commun.* **2022**, *13* (1), 949. https://doi.org/10.1038/s41467-022-28543-x.
(12) Fung, V.; Ganesh, P.; Sumpter, B. G. Physically Informed Machine Learning Prediction of Electronic Density of States. *Chem. Mater.* **2022**. https://doi.org/10.1021/acs.chemmater.1c04252.
(13) Xie, T.; Grossman, J. C. Crystal Graph Convolutional Neural Networks for an Accurate and Interpretable Prediction of Material Properties. *Phys. Rev. Lett.* **2018**, *120* (14), 145301. https://doi.org/10.1103/PhysRevLett.120.145301.
(14) Kresse, G.; Hafner, J. Ab Initio Molecular Dynamics for Liquid Metals. *Phys. Rev. B* **1993**, *47* (1), 558–561. https://doi.org/10.1103/PhysRevB.47.558.
(15) Kresse, G.; Furthmüller, J. Efficiency of Ab-Initio Total Energy Calculations for Metals and Semiconductors Using a Plane-Wave Basis Set. *Comput. Mater. Sci.* **1996**, *6* (1), 15–50. https://doi.org/10.1016/0927-0256(96)00008-0.
(16) Kresse, G.; Furthmüller, J. Efficient Iterative Schemes for Ab Initio Total-Energy Calculations Using a Plane-Wave Basis Set. *Phys. Rev. B* **1996**, *54* (16), 11169–11186. https://doi.org/10.1103/PhysRevB.54.11169.
(17) Seh, Z. W.; Kibsgaard, J.; Dickens, C. F.; Chorkendorff, I.; Nørskov, J. K.; Jaramillo, T. F. Combining Theory and Experiment in Electrocatalysis: Insights into Materials Design. *Science* **2017**, *355* (6321), eaad4998. https://doi.org/10.1126/science.aad4998.
(18) *Analysis of Acid-Stable and Active Oxides for the Oxygen Evolution Reaction*. https://doi.org/10.1021/acsenergylett.0c02030.
(19) Meng, Y.; Song, W.; Huang, H.; Ren, Z.; Chen, S.-Y.; Suib, S. L. Structure–Property Relationship of Bifunctional MnO2 Nanostructures: Highly Efficient, Ultra-Stable Electrochemical Water Oxidation and Oxygen Reduction Reaction Catalysts Identified in Alkaline Media. *J. Am. Chem. Soc.* **2014**, *136* (32), 11452–11464. https://doi.org/10.1021/ja505186m.
(20) Tarascon, J.-M.; Armand, M. Issues and Challenges Facing Rechargeable Lithium Batteries. *Nature* **2001**, *414* (6861), 359–367. https://doi.org/10.1038/35104644.

(21) Minh, N. Q. Ceramic Fuel Cells. *J. Am. Ceram. Soc.* **1993**, *76* (3), 563–588. https://doi.org/10.1111/j.1151-2916.1993.tb03645.x.
(22) Bachman, J. C.; Muy, S.; Grimaud, A.; Chang, H.-H.; Pour, N.; Lux, S. F.; Paschos, O.; Maglia, F.; Lupart, S.; Lamp, P.; Giordano, L.; Shao-Horn, Y. Inorganic Solid-State Electrolytes for Lithium Batteries: Mechanisms and Properties Governing Ion Conduction. *Chem. Rev.* **2016**, *116* (1), 140–162. https://doi.org/10.1021/acs.chemrev.5b00563.
(23) Ong, S. P.; Mo, Y.; Richards, W. D.; Miara, L.; Lee, H. S.; Ceder, G. Phase Stability, Electrochemical Stability and Ionic Conductivity of the Li10±1MP2X12 (M = Ge, Si, Sn, Al or P, and X = O, S or Se) Family of Superionic Conductors. *Energy Environ. Sci.* **2012**, *6* (1), 148–156. https://doi.org/10.1039/C2EE23355J.
(24) Masias, A.; Marcicki, J.; Paxton, W. A. Opportunities and Challenges of Lithium Ion Batteries in Automotive Applications. *ACS Energy Lett.* **2021**, *6* (2), 621–630. https://doi.org/10.1021/acsenergylett.0c02584.
(25) Aravindan, V.; Gnanaraj, J.; Lee, Y.-S.; Madhavi, S. LiMnPO4 – A next Generation Cathode Material for Lithium-Ion Batteries. *J. Mater. Chem. A* **2013**, *1* (11), 3518–3539. https://doi.org/10.1039/C2TA01393B.
(26) Wani, T. A.; Suresh, G. A Comprehensive Review of LiMnPO4 Based Cathode Materials for Lithium-Ion Batteries: Current Strategies to Improve Its Performance. *J. Energy Storage* **2021**, *44*, 103307. https://doi.org/10.1016/j.est.2021.103307.
(27) Lee, K.-J.; Kang, L.-S.; Uhm, S.; Yoon, J. S.; Kim, D.-W.; Hong, H. S. Synthesis and Characterization of LiMnBO3 Cathode Material for Lithium Ion Batteries. *Curr. Appl. Phys.* **2013**, *13* (7), 1440–1443. https://doi.org/10.1016/j.cap.2013.04.027.
(28) Ragupathi, V.; Safiq, M.; Panigrahi, P.; Hussain, T.; Raman, S.; Ahuja, R.; Nagarajan, G. S. Enhanced Electrochemical Performance of LiMnBO3 with Conductive Glassy Phase: A Prospective Cathode Material for Lithium-Ion Battery. *Ionics* **2017**, *23* (7), 1645–1653. https://doi.org/10.1007/s11581-017-2019-8.
(29) Qiu, H.; Jin, D.; Wang, C.; Chen, G.; Wang, L.; Yue, H.; Zhang, D. Design of Li2FeSiO4 Cathode Material for Enhanced Lithium-Ion Storage Performance. *Chem. Eng. J.* **2020**, *379*, 122329. https://doi.org/10.1016/j.cej.2019.122329.